DNA nanoswitches: a quantitative platform for gel-based biomolecular interaction analysis

Mounir A Koussa[1,6], Ken Halvorsen[2,3,6], Andrew Ward[3] & Wesley P Wong[3–5]

We introduce a nanoscale experimental platform that enables kinetic and equilibrium measurements of a wide range of molecular interactions using a gel electrophoresis readout. Programmable, self-assembled DNA nanoswitches serve both as templates for positioning molecules and as sensitive, quantitative reporters of molecular association and dissociation. We demonstrated this low-cost, versatile, 'lab-on-a-molecule' system by characterizing ten different interactions, including a complex four-body interaction with five discernible states.

Gel electrophoresis has been a workhorse of biological research for over 50 years, providing a simple way to determine size, topology and quantity of DNA, RNA and protein[1–3]. However, quantitative kinetic and thermodynamic characterization of molecular interactions on gels remains a challenge. For example, electrophoretic mobility shift assays are primarily used for qualitative analysis of protein–nucleic acid interactions[4]. Quantitative biomolecular interaction analysis typically requires specialized techniques such as surface plasmon resonance (SPR) (for example, Biacore), radiolabeling or isothermal titration calorimetry (ITC), with cost, necessary technical expertise and material requirements sometimes posing barriers to their use (**Supplementary Table 1**). Furthermore, quantitative analysis of long-lived interactions, small-molecule interactions and multicomponent complexes are difficult even with these advanced approaches.

We introduce an instrument-free platform, based on DNA self-assembly[5–7], that meets these challenges by enabling quantitative analysis of molecular interactions using standard gel electrophoresis, for pennies per sample (**Supplementary Table 1**). DNA oligonucleotides (60 nt) are functionalized with interacting molecules and hybridized to specific locations on an ssDNA scaffold (M13mp18, 7,249 nt) to form DNA nanoswitches. These nanoswitches report molecular associations and dissociations through induced topological changes. Because DNA can be separated on the basis of topology[8], the different interaction states can be easily resolved as distinct bands on a gel (**Fig. 1a**).

These nanoswitches have several useful features. Their programmable nature enables precise control over relative concentrations and stoichiometries on a per-molecule basis. The large DNA construct causes interaction-triggered topological changes to yield distinct and repeatable gel shifts, even with the integration of large proteins[5]. Additionally, the large size of the DNA allows for the incorporation of thousands of dye molecules, thereby dramatically amplifying the signal per interaction and making readout of the nanoswitches orders of magnitude more sensitive than with most other techniques (**Supplementary Table 1**). Together these features make DNA nanoswitches a versatile, accessible and inexpensive tool for studying multimolecular interactions.

By monitoring changes in the nanoswitch states over time, we can determine equilibrium and kinetic rate constants for a variety of molecular systems using standard gel electrophoresis. Loop closure over time is used to determine association rate constants, whereas loop opening over time, in the presence of a competitor, is used to determine the dissociation rate constant (**Fig. 1b**,**c** and **Supplementary Fig. 1**). These kinetic processes take place in solution and are 'quenched' to halt kinetics at various time points, with the gel acting as a post-experiment readout, enabling experimental conditions that are independent of gel running conditions. Ease of readout and other nanoswitch characteristics can be optimized by tuning key design parameters, including oligonucleotide length, ligand positioning, reaction concentrations and temperatures (Online Methods).

We first assessed the nanoswitch platform using the ubiquitous biotin-streptavidin system. At physiological salt conditions and 25 °C, we measured a dissociation time of 9.7 ± 0.4 days (all values are reported as the error-weighted fit parameter ± its 1σ confidence interval), closely matching previously reported values[9]. To demonstrate parallel exploration of a broad range of experimental conditions, we obtained off-rates at 16 different conditions by measuring the fraction dissociated at six time points per condition and running all 96 samples on a single gel (**Supplementary Fig. 2**). Each condition showed exponential decay over time, yielding 16 uniquely determined off-rates ranging from 0.8 h to 3 months with an uncertainty typically <10% (**Supplementary Fig. 2** and **Supplementary Table 2**). Dissociation kinetics varied nearly 1,000-fold over our temperature range (4–50 °C) but only about twofold over our salt range (25–500 mM) (**Fig. 1d** and **Supplementary Fig. 3**). On the basis of these results, we present

[1]Program in Neuroscience, Department of Neurobiology, Harvard Medical School, Boston, Massachusetts, USA. [2]The RNA Institute, University at Albany, Albany, New York, USA. [3]Program in Cellular and Molecular Medicine, Boston Children's Hospital, Boston, Massachusetts, USA. [4]Department of Biological Chemistry and Molecular Pharmacology, Harvard Medical School, Boston, Massachusetts, USA. [5]Wyss Institute for Biologically Inspired Engineering, Harvard University, Boston, Massachusetts, USA. [6]These authors contributed equally to this work. Correspondence should be addressed to K.H. (khalvorsen@albany.edu) or W.P.W. (wesley.wong@childrens.harvard.edu).

RECEIVED 6 MAY; ACCEPTED 17 OCTOBER; PUBLISHED ONLINE 8 DECEMBER 2014; DOI:10.1038/NMETH.3209

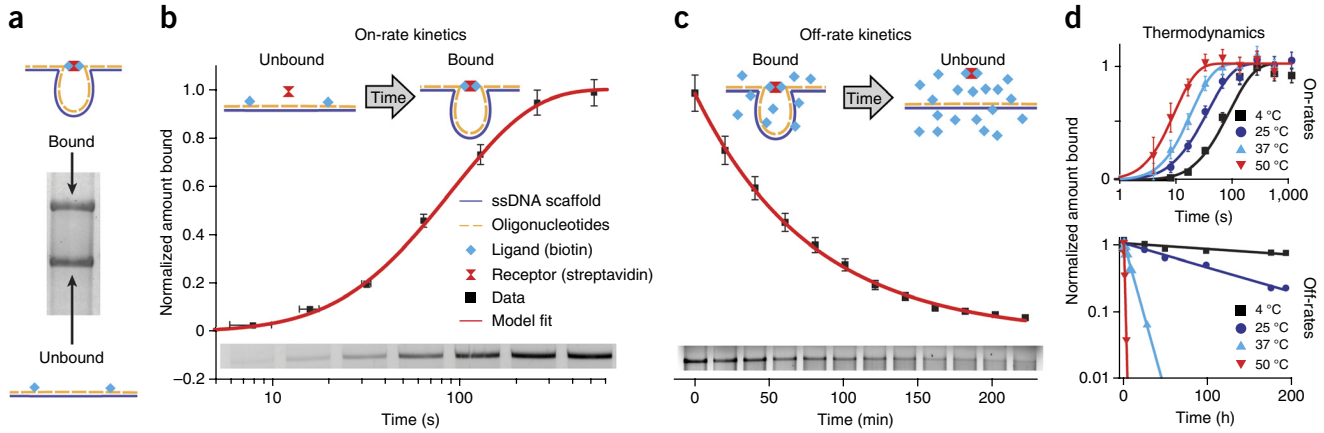

Figure 1 | Kinetic measurements using DNA nanoswitches. (**a**) The two states (bound and unbound) of the DNA nanoswitches can be distinguished by gel electrophoresis. (**b**) With two biotins integrated into the nanoswitch, loop formation begins when unlabeled streptavidin is introduced and progresses over time as evidenced by increasing intensity in the bound (looped) band across different lanes of a gel (bottom). The growth curve is fit with a kinetic model to determine the on-rate. (**c**) Addition of excess biotin blocks loop formation, making bond rupture irreversible, which leads to the exponential decay of nanoswitches from the bound state to the unbound state, as shown by the decreasing intensity in the unbound band across different lanes of a gel (bottom). (**d**) Temperature dependence of on-rates and off-rates for the biotin-streptavidin interaction at 150 mM NaCl. Horizontal error bars (**b**) represent uncertainty in mixing time (±2 s), and vertical error bars indicate ±7% uncertainty in the intensity (1σ confidence interval determined from 48 repeated measurements of the same construct; see "Data analysis" in the Online Methods).

a semi-empirical model for dissociation kinetics between streptavidin and biotin-labeled oligonucleotides from 25 to 50 °C and 25 to 500 mM NaCl:

$$k_{off} \approx Te^{\left(42.4 - \frac{18{,}300}{T} - 0.033\sqrt{I}\right)}$$

where k_{off} is the value of the off-rate in s^{-1}, T is the value of the absolute temperature in kelvin, and I is the value of the ionic strength of the solution in micromolar concentration (Online Methods and **Supplementary Fig. 3d**). This model does not describe the behavior at 4 °C, presumably owing to temperature-dependent changes in heat capacity[10].

We measured on-rate kinetics for the biotin-streptavidin interaction, at a variety of temperatures, by monitoring loop formation over time. Loop closure occurs through two separate binding events: the binding of a molecule from solution to the nanoswitch and then the closing of the loop. Thus, we fit loop-closure data to a two-step kinetic model to extract these rates (**Fig. 1b**,**d**, Online Methods, **Supplementary Table 3** and **Supplementary Fig. 1**). At 150 mM salt, we measured a room-temperature (25 °C) on-rate of $(4.0 \pm 0.7) \times 10^6$ M^{-1} s^{-1}. Combining our on-rate and off-rate measurements, we calculated a dissociation constant of $(2.94 \pm 0.51) \times 10^{-13}$ M, an equilibrium free energy change, ΔG^0, of -17.1 ± 0.1 kcal mol^{-1} and an equilibrium enthalpy change, ΔH, of 26.01 ± 0.05 kcal mol^{-1} (**Supplementary Table 3**). In general, our measurements are consistent with values reported in the literature (**Supplementary Table 2**). Specifically, we are within 15% of the reported off-rate of a biotin-labeled oligonucleotide[9], within 30% of on-rate measurements from SPR[11] and within 5% of both equilibrium ΔH measurements by ITC[12] and equilibrium ΔG measurements made by monitoring kinetics of radiolabeled biotin[13].

Without modifying the DNA construct, we were also able to measure kinetic and equilibrium properties for avidin and NeutrAvidin (**Supplementary Table 3**). Although NeutrAvidin's affinity for biotin was 20 times weaker than avidin's, they surprisingly had similar off-rates, a result underscoring the limitation of relying solely on affinity measurements to characterize an interaction.

To demonstrate the ability to measure weaker interactions, we incorporated desthiobiotin, a biosynthetic precursor to biotin that binds streptavidin with far lower affinity, into our nanoswitch[14]. By optimizing gel running conditions, we resolved the looped and unlooped constructs in as little as 6 min, measuring the off-rate of streptavidin-desthiobiotin as 35.3 ± 7.5 min at 4 °C and 8.6 ± 1.2 min at room temperature (**Supplementary Fig. 4**). We note that although the system is ideal for quantification of long-lived interactions, even those out of the range of SPR, the time required to resolve the bands in a gel currently sets the lower limit of detectable dissociation lifetimes to minutes.

The modularity of the DNA nanoswitch facilitates the easy incorporation of different types of molecules. We exploited this feature to measure several biologically relevant interactions including a covalent bond taking weeks to dissociate (**Fig. 2a**), a protein–small-molecule interaction dissociating over days (**Fig. 2b**), an antibody-antigen interaction taking hours to dissociate at room temperature (**Fig. 2c**) and a 20-bp DNA oligonucleotide dissociating over hours at 50 °C (**Fig. 2d**). Additionally, we were able to study peptide ligation kinetics with a time constant of minutes (**Fig. 2e**) and restriction enzyme cleavage over seconds (**Fig. 2f**). As with many techniques including SPR, assay preparation requires the derivatization of at least one molecule of interest. Here, we attached our molecules of interest to a DNA oligonucleotide, which can be accomplished using a variety of techniques. In addition to sulfosuccinimidyl-4-(*N*-maleimidomethyl)cyclohexane-1-carboxylate cross-linking[5], we previously described the use of click chemistry to attach peptides to oligonucleotides and the use of the enzyme sortase[15] to rapidly and efficiently attach proteins to our nanoswitches while preserving protein function[16].

The platform's versatility is facilitated by its universal gel readout. An extreme example of this is our characterization of the

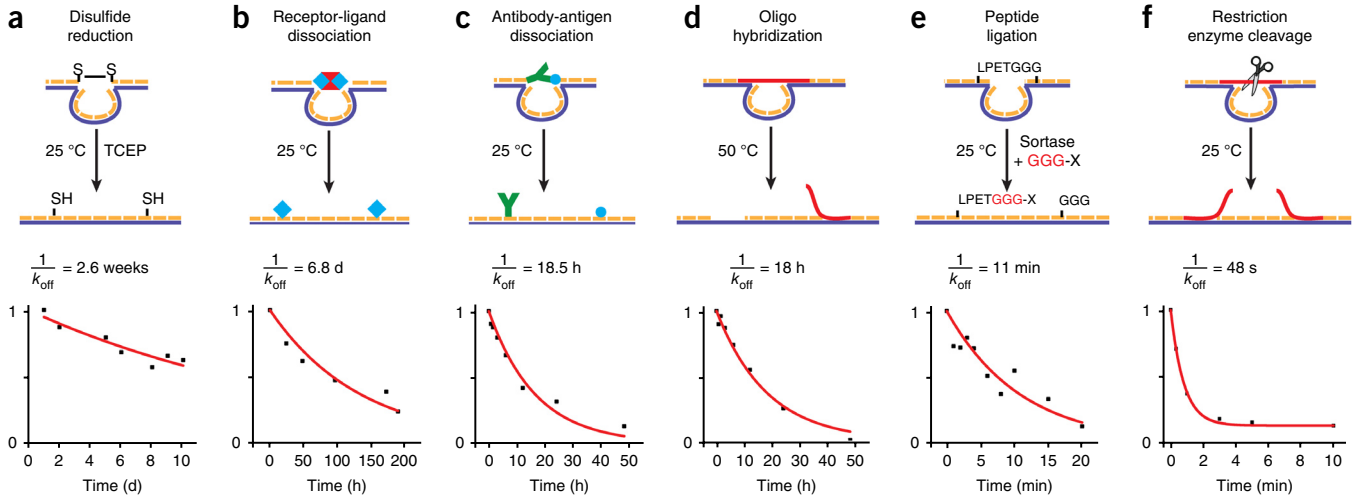

Figure 2 | Various biological measurements using the nanoswitch platform. Schematic representation of each measurement are shown, with data and model fit beneath. (**a**) Disulfide-bond reduction in 10 μM TCEP at room temperature (k_{off} = 2.6 ± 0.4 weeks). (**b**) Biotin-streptavidin dissociation in 300 mM NaCl at room temperature (k_{off} = 6.8 ± 0.8 d). (**c**) Dissociation kinetics of digoxigenin and its antibody at room temperature (k_{off} = 18.5 ± 2.0 h). (**d**) Melting kinetics of a 20-nt oligonucleotide at 50 °C (k_{off} = 18 ± 1.6 h). (**e**) Sortase-catalyzed transpeptidation at room temperature ($k_{ligation}$ = 11 ± 1.3 min). (**f**) XhoI restriction enzyme kinetics at room temperature (k_{cut} = 48 ± 2 s). Each value is reported as an error-weighted fit parameter plus or minus its 1σ confidence interval.

reduction of a disulfide bond at 25 °C in 10 μM TCEP (Tris(2-carboxyethyl)phosphine) yielding a time constant of 2.6 ± 0.4 weeks (**Fig. 2a**). Because the signal per molecule is dependent on only the nanoswitch size, this two-atom system yielded the same level of signal per interaction as a 150-kDa antibody binding to its antigen (**Fig. 2c**).

Additionally, the programmability of these nanoswitches enables multiple topological states to be individually distinguished on a gel, thereby facilitating the analysis of complex multicomponent interactions (**Fig. 3**). We engineered nanoswitches with three integrated ligands, placed strategically to form two asymmetric loops when simultaneously bound by a bispecific receptor. The resulting nanoswitch adopted five resolvable states that could be identified with control experiments (**Fig. 3a** and **Supplementary Fig. 5**). We measured bidirectional transitions for all five states, thus determining all rate constants (**Fig. 3**, **Supplementary Figs. 6** and **7** and **Supplementary Table 4**). This ability to monitor the fraction of molecules populating each state over time would be difficult or impossible to achieve with most other measurement techniques.

Our approach enables low-cost, accessible and parallel multicomponent biomolecular interaction analysis using a basic laboratory technique, gel electrophoresis. We have demonstrated our platform's ability to characterize interactions with time constants ranging from seconds to months (approximately six orders of magnitude), for a wide variety of molecular interactions, temperatures and buffer conditions. The signals were robust and highly amplified, giving detection limits in the range of attomoles and

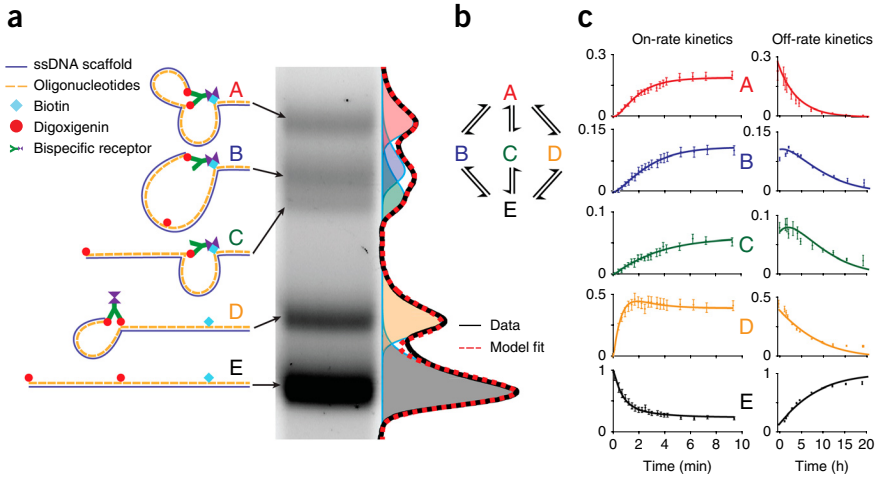

Figure 3 | Multistate kinetic analysis. (**a**) A nanoswitch functionalized with two digoxigenin molecules and one biotin molecule can adopt five discernible states upon addition of a bispecific receptor. All five topological states, A–E (**Supplementary Fig. 6**), can be resolved within a single lane of an agarose gel. These bands can be fit globally with a single fit of a sum of skewed Gaussian curves. The black curve represents the median pixel intensity, the dashed red curve represents the fit that is the sum of five skewed Gaussians, and the individual skewed Gaussians are shaded by state. (**b**) Reaction diagram illustrating the possible transitions between each of the five states. (**c**) Left, on-rate measurements indicating the value of each state at 20 different time points. Solid curves indicate the result of a global fit of all states to the kinetic model illustrated in **b**. Right, off-rate measurements indicating the value of each state at 12 different time points. Solid curves indicate the result of a global fit of all states to the kinetic model illustrated in **b**. These fits taken together allowed for the determination of all rate constants from 32 lanes, which can be run on a single gel (**Supplementary Fig. 7** and **Supplementary Table 4**). Error bars are based on 1σ confidence intervals of the least-squares fit to each band (see "Gel image analysis" in the Online Methods). The on-rate model was fit using 100 measurements; the off-rate model was fit using 60 measurements.

allowing quantitative kinetic and thermodynamic analysis of proteins as shown here with femtomoles of material (~1 ng for a 50-kDa protein). In contrast to other techniques that provide one signal to analyze (for example, SPR, radiolabeling and ITC), our technique has the ability to perform independent measurement of five signals simultaneously, allowing complete characterization of a complex five-state system. The modularity and programmability of the nanoswitches affords control over the relative concentrations and stoichiometries of interacting components, independent of the nanoswitch concentration. This feature suggests that, in addition to monitoring reactions, nanoswitches could be used as a template-directed synthesis technique to control complex reactions. Overall, this unique lab-on-a-molecule platform will be a powerful research tool, accessible to anyone able to perform gel electrophoresis.

METHODS

Methods and any associated references are available in the online version of the paper.

Note: Any Supplementary Information and Source Data files are available in the online version of the paper.

ACKNOWLEDGMENTS

The authors gratefully acknowledge D. Corey, G. Yellen, R. Wilson, J. Holt, H. Ploegh, G. Wong, A. Badran, Z. Tsun, A. Golden and members of the Wong and Corey Labs for critical discussions and T. Kao for her early work on the project. Funding for this project was provided by US National Institutes of Health R01 DC02281 to D. Corey; M.A.K. was supported by National Science Foundation USA GRFP 2012147612; W.P.W. was supported by Boston Children's Hospital startup funds and Takeda New Frontier Science.

AUTHOR CONTRIBUTIONS

The initial idea was conceived by K.H. and W.P.W. Experiments were designed by all authors. The method was expanded by M.A.K. and A.W., and experiments were carried out by K.H., M.A.K. and A.W. All authors participated in data analysis, critical discussion and writing of the manuscript.

COMPETING FINANCIAL INTERESTS

The authors declare competing financial interests: details are available in the online version of the paper.

1. Thorne, H.V. *Virology* **29**, 234–239 (1966).
2. Bishop, D.H.L., Claybrook, J.R. & Spiegelman, S. *J. Mol. Biol.* **26**, 373–387 (1967).
3. Smithies, O. *Biochem. J.* **61**, 629–641 (1955).
4. Hellman, L.M. & Fried, M.G. *Nat. Protoc.* **2**, 1849–1861 (2007).
5. Halvorsen, K., Schaak, D. & Wong, W.P. *Nanotechnology* **22**, 494005 (2011).
6. Saccà, B. & Niemeyer, C.M. *Angew. Chem. Int. Ed. Engl.* **51**, 58–66 (2012).
7. Seeman, N.C. *Annu. Rev. Biochem.* **79**, 65–87 (2010).
8. Aaij, C. & Borst, P. *Biochim. Biophys. Acta* **269**, 192–200 (1972).
9. Levy, M. & Ellington, A.D. *Chem. Biol.* **15**, 979–989 (2008).
10. Prabhu, N.V. & Sharp, K.A. *Annu. Rev. Phys. Chem.* **56**, 521–548 (2005).
11. Qureshi, M.H., Yeung, J.C., Wu, S.C. & Wong, S.L. *J. Biol. Chem.* **276**, 46422–46428 (2001).
12. Klumb, L.A., Chu, V. & Stayton, P.S. *Biochemistry* **37**, 7657–7663 (1998).
13. Chivers, C.E. *et al. Nat. Methods* **7**, 391–393 (2010).
14. Florin, E.L., Moy, V.T. & Gaub, H.E. *Science* **264**, 415–417 (1994).
15. Chen, I., Dorr, B.M. & Liu, D.R. *Proc. Natl. Acad. Sci. USA* **108**, 11399–11404 (2011).
16. Koussa, M.A., Sotomayor, M. & Wong, W.P. *Methods* **67**, 134–141 (2014).

ONLINE METHODS

We provide a **Supplementary Protocol** that includes lists of reagents needed and detailed step-by-step instructions for performing on-rate and off-rate experiments. Additionally, to facilitate getting started, materials will be available upon request as detailed in section 2 of the **Supplementary Protocol**.

General nanoswitch formation. The nanoswitches were constructed as previously described in detail[5]. Circular ssDNA from the 7,249-nt bacteriophage M13 (New England BioLabs) was linearized by enzymatic cleavage of a single site using BtscI (New England BioLabs) and a site-specific oligonucleotide. Oligonucleotides (from Bioneer or Integrated DNA Technologies (IDT)) were designed to complement the linearized M13 DNA along the backbone, resulting in 120 60-nt oligonucleotides and a single 49-nt oligonucleotide. The first and last oligonucleotide along with ten evenly distributed oligonucleotides are intended to be interchangeable and will be referred to as variable oligonucleotides (var 1–12, with var 1 representing the first oligonucleotide and var 12 representing the last oligonucleotide—see **Supplementary Protocol**, **Supplementary Data** and **Supplementary Tables 5** and **6**). These variable oligonucleotides were stored separately from the remaining 109, referred to as backbone (bb) oligonucleotides, which were mixed in equimolar concentration in a single tube. Mixing a molar excess of the oligonucleotides (10:1 unless otherwise noted) with the ssDNA scaffold and subjecting the mixture to a temperature ramp (from 90 to 20 °C at 1 °C min^{-1} unless otherwise noted) produced dsDNA. Final constructs were spiked with a low concentration of DNA ladder (BstNI digest of pBR322 DNA, New England BioLabs) to aid in quantification. For many experiments the constructs were PEG precipitated after annealing to remove excess oligonucleotides. The PEG precipitation was performed as described in section 3.3 of the **Supplementary Protocol** and as previously described in ref. 16.

Key design considerations. The nanoswitches were designed with several key design considerations to ensure that they function properly and robustly over a wide range of conditions. The oligonucleotide length was selected to be 60 nt to ensure both site specificity and that the oligonucleotides would not spontaneously fall off even at temperatures as high as 50 °C. At 50 °C, even a 20-mer oligonucleotide has a long lifetime of ~18 h (**Fig. 2d**), and the lifetime of a 60-mer oligonucleotide is predicted to be orders of magnitude longer than that of the 20-mer oligonucleotide[17].

The ligands were positioned at locations that allow for easy resolution of the looped and unlooped bands. Placement of the oligonucleotides on variable regions 4 and 5 yields two bands that are quite close to one another under our standard gel running conditions. The further apart the ligands are, the more easily resolvable the two bands become. The spacing of ligands on the DNA scaffold also controls their effective concentration, with the effective concentration of one ligand to the other generally decreasing as they are spaced further apart (though if the ligands are brought within one persistence length of the polymer, the effective concentration may decrease dramatically). We have found that the use of variable regions 4 and 8 provides a nice middle ground (**Supplementary Table 7**).

There are three concentrations that can be independently tuned in an on-rate experiment. There is the concentration of the scaffold, the concentration of the receptor, and the effective concentration between the two ligands on the polymer. If these concentrations are adjusted carefully, many problems can be avoided. For example, if the effective concentration between the two tethered ligands is significantly higher than the concentration of the receptor, then one can minimize capping (the binding of two receptors to a single scaffold resulting in an unloopable construct). We note, however, that because our model accounts for capping, the values obtained outside this optimal regime will still be correct; the looped-band intensities will simply be weaker, resulting in a lower signal-to-noise ratio. Although not usually a problem, one can avoid higher order aggregation by ensuring that the scaffold concentration is significantly lower than the effective concentration between the two ligands on the scaffold. One can also simplify the analysis by selecting a receptor concentration that is significantly higher than the scaffold concentration so that the receptor concentration stays effectively constant over the course of the experiment. Following these experimental design principles, in our experiments using variable oligonucleotides 4 and 8, the effective concentration between the two ligands on the loop is ~30 nM, the scaffolds are used at a concentration of 80 pM, and the receptor is used at a nominal concentration of 3 nM (**Supplementary Table 8**).

In addition to the ratio of concentrations, there are some important lower and upper limits of concentration to keep in mind. We have found that working with protein concentrations below 1 nM can be unreliable owing to losses of protein to the walls of the tubes. We have performed on-rate experiments with streptavidin concentrations as low as 0.3 nM, but losses of protein can be as high as 80% even in protein LoBind tubes (Eppendorf technical data sheet). Unless a means of eliminating protein loss to tubes and pipette tips is implemented, we do not recommend working below 1 nM. The upper limit is not a hard limit. We have found that the on-rate for streptavidin is very fast at 30 nM, making it difficult to pipette fast enough to take multiple time points before the plateau. If one has a means of more rapidly mixing solutions (i.e., microfluidics), or a protein with a slower on rate, higher protein concentrations can be used. We have found that 3 nM provides a nice middle ground, though one may wish to optimize the protein concentration used according to the speed of mixing and the solution on-rate of the protein being studied.

Following these design principles and those laid out in ref. 5 is key to the successful use of this platform. The **Supplementary Protocol** provides information on reagents needed and detailed step-by-step instructions on how to successfully perform on-rate and off-rate experiments.

Electrophoretic conditions. All looped constructs were run in 0.7% agarose gels, cast from LE agarose (Seakem) or Ultrapure Agarose (Life Technologies) dissolved in 0.5× Tris-borate EDTA (TBE) (Bio-Rad). Before loading, samples were mixed with a Ficoll-based loading solution (Promega), which we found to give sharper bands than glycerol-based loading dyes, simplifying quantification. Gels were run for 90–100 min at 4 V cm^{-1}, unless otherwise noted, and subsequently stained in 1× SYBRGold stain (Invitrogen) for a minimum of 30 min before being imaged with

a gel imager (Bio-Rad) or laser gel-scanner (GE Typhoon). It is important to note that the standard output file of this imager is often set to a .gel file, which has a nonlinear intensity scaling. Such .gel images can be linearized using the ImageJ "Linearize GelData" plug-in (http://rsb.info.nih.gov/ij/plugins/linearize-gel-data.html). Alternatively, the gel image can be saved as a linear .tiff file off of the imager. We would like to point out that these expensive imagers are not required for quantification, and we obtained similar results using a blue transilluminator (Invitrogen) and a point-and-shoot camera (Canon S95).

Biotin-streptavidin nanoswitch experiments. This construct used biotinylated versions of two oligonucleotides (var 4 and var 8), which were used in 4× molar excess to the scaffold, and all other oligonucleotides were used in a 10× molar excess. The reason for this lesser amount is twofold: (i) to be less wasteful of the more expensive functionalized oligonucleotides and (ii) because excess biotin oligonucleotide in solution could interfere with our measurements. The final DNA construct was then diluted 100× from its original concentration of ~16 nM (to 160 pM) and mixed in equal volumes with streptavidin (Rockland) at 6 nM nominal concentration to form the loops, yielding final nominal scaffold and streptavidin concentrations of ~80 pM and 3 nM, respectively.

On-rate experiments were performed by mixing equal volumes of 160 pM DNA construct with a nominal 6 nM streptavidin concentration, followed by taking 10-μL aliquots of the mixture at various times and mixing them with 1 μL of a saturated biotin solution to quench the formation of loops. The 25 °C experiment was performed at room temperature, the 4 °C experiment was performed in a cold room, and the 37 °C and 50 °C experiments were performed using a thermal cycler. For on-rate experiments, using low-binding tubes (Eppendorf LoBind) was important for getting repeatable results owing to significant streptavidin adsorption to the tubes when incubated at 6 nM. Actual concentrations used to determine the on-rates were measured using spectrophotometry and a HABA assay to determine streptavidin activity. We found that the actual streptavidin concentration was within 10% of the nominal concentration, and over 85% of the protein was active on the basis of the HABA assay.

Off-rate measurements were performed by forming looped construct as described above and letting the solution sit for at least 24 h to allow the system to reach equilibrium. Aliquots of the looped construct were mixed at various times with a quenching solution consisting of biotin and sodium chloride to achieve the proper experimental salt concentrations and were immediately put at the experimental temperature. The 4 °C condition was done in a refrigerator, the 25 °C sample was done in a water bath, and the 37 °C and 50 °C temperatures were done in a thermal cycler. To run all the samples on a single gel, the quenching times were determined relative to the predetermined gel running time.

Preparations with avidin and NeutrAvidin were prepared in the same way, but protein concentrations were sometimes altered to enable on-rate measurements over a similar timescale to that of the streptavidin experiments.

Desthiobiotin-streptavidin. Desthiobiotin experiments were conducted in a similar manner to the biotin experiments with slight modifications. The var 4 oligonucleotide was changed to a desthiobiotin-functionalized oligonucleotide, whereas the var 8 oligonucleotide remained biotin functionalized. The off-rate of the desthiobiotin interaction is much faster than the typical 100-min gel run time. Noting that once a loop opens in the gel, the reptation of the DNA prevents the loop from closing again, we ran samples for different amounts of time in the gel at 15 V cm^{-1} and 4 °C and quantified the fraction looped as a function of running time (**Supplementary Fig. 4**). In addition to allowing the determination of the desthiobiotin-streptavidin off-rate, this gel also allowed us to determine the minimum amount of time required to achieve separation of the looped and unlooped bands in the gel. This enabled the use of the standard quenching technique for measuring desthiobiotin off-rates as described in the previous section; these gels were run at 15 V cm^{-1} for 10 min in prechilled electrophoresis buffer.

DNA hybridization experiments. This construct used a 50-nt 'bridge' oligonucleotide to span the last 30 nt of the var 4 region and the first 20 nt of the var 8 region. Thus, the normal var 4 and var 8 oligonucleotides were omitted from the mixture and replaced with three oligonucleotides: the aforementioned bridge oligonucleotide and two small 'filler' oligonucleotides to fill the remaining bases so that the M13 scaffold would be fully hybridized. In this case, the bridge oligonucleotide was added in equimolar concentration with the scaffold strand, whereas the other oligonucleotides remained at 10× molar excess. Off-rate measurements were quenched with 500 nM 20-nt oligonucleotide corresponding to the loop-closure site. Kinetics were accelerated by performing the measurement at 50 °C.

Enzyme cleavage experiments. These constructs were made as described above but with a bridge oligonucleotide containing an inserted sequence recognized by the XhoI enzyme (New England BioLabs). The complement to this restriction sequence was also added to ensure that this region was double-stranded. Cleavage measurements were performed by adding enzyme to the loops (with final concentrations of 2.2 nM and 1,000 units mL^{-1} for the loops and enzyme, respectively) in the recommended buffer (New England BioLabs) and quenching the enzyme activity with 75 mM EDTA at various times at room temperature.

Antibody-antigen experiments. This construct used a 3′ digoxigenin–labeled version of the var 8 oligonucleotide (Integrated DNA Technologies) and a 5′ anti-dig–labeled version of the var 4 oligonucleotide. The antibody-labeled oligonucleotide was made by chemically cross-linking a free amine on the antibody (polyclonal sheep antibody from Roche) to a thiol-labeled oligonucleotide and purified by electroelution as described previously[5]. The construct was made with two annealing steps. First, all the oligonucleotides with the exception of the antibody-labeled oligonucleotide were mixed with the scaffold strand and annealed following our standard protocol described above (except a 1:1, rather than 10:1, molar ratio was used for the digoxigenin oligonucleotide). Second, the purified antibody oligonucleotide was added in a 1:1 molar ratio and annealed from 37 °C to 4 °C at 0.5 °C min^{-1} to facilitate annealing of the antibody-modified var 4 oligonucleotide. Off-rate measurements were performed by quenching with 335 nM of antibody at various times at room temperature.

doi:10.1038/nmeth.3209

Sortase-catalyzed peptide ligation experiments. This construct was created in three steps. (1) Var 4 and var 5 oligonucleotides with a 3′ and a 5′ azide, respectively, were functionalized with sortase-compatible peptides. (2) These two oligonucleotides were linked together with sortase. (3) The peptide-bridged oligonucleotides were hybridized onto the DNA nanoswitch. All custom peptides were purchased from NeobioLab.

1. To create the sortase-compatible oligonucleotides, sortase-compatible peptides were covalently attached using click chemistry as previously descroned[16]. Pra-LPETGHHHHHH, where Pra is a propargyl glycine, which adds an alkyne functionality, was coupled to var 4–azide using copper-catalyzed click chemistry. Azide–var 5 was then functionalized with a Flag-TEV-GGG-Pra peptide, where Flag denotes a Flag tag and TEV denotes a cleavage site for the tobacco etch virus protease. After the click chemistry the oligonucleotides were processed with a Qiagen nucleotide-removal kit and run on a polyacrylamide gel. The bands corresponding to the peptide-oligonucleotide chimeras were cut out, and the products were extracted via electroelution as previously described.
2. Once purified, the Flag-TEV-GGG-var 5 was treated with TEV (Sigma) and the two oligonucleotides were concentrated as previously described[16]. These oligonucleotides were then at a concentration of ~10 μM as judged by running on a precast 4–20% gradient polyacrylamide TBE gel (Bio-Rad). Equal volumes (10 μL each) of the sortase-compatible oligonucleotides were mixed with 5 μL of 14.1 mg mL^{-1} sortase[15], and 25 μL of 2× sortase reaction buffer (600 mM Tris-HCl, pH 7.5, 300 mM NaCl, 10 mM $MgCl_2$, and 10 mM $CaCl_2$). This was allowed to sit for 3 h at room temperature before we ran it on a polyacrylamide gel and purified the dimer band via electroelution, yielding var 4-LPETGGG-var 5. (Note that the GGG indicates the amino acid string Gly-Gly-Gly.)
3. The var 4-LPETGGG-var 5 was used instead of the normal var 4 and var 5. This was annealed onto the linear M13 backbone at a 1:1 ratio and was added along with the other oligonucleotides at the beginning of the annealing, as peptide denaturation was not a concern. This yielded loops with the peptide LPETGGG bridging variable regions 4 and 5.

With these loops in hand, we could observe loop opening as a result of sortase ligating free GGG-X peptide. To accomplish this, we made a mixture with the following concentrations. 2 nM DNA nanoswitches, 10 μM sortase, 40 μM GGG-S-S-CH_3, 300 mM Tris-HCl, pH 7.5, 150 mM NaCl, 5 mM $CaCl_2$, and 5 mM $MgCl_2$. Catalysis by sortase is highly calcium dependent; thus, the transpeptidation could be quenched at different times by adding an equal volume of 100 mM EDTA in water. Ten time points were collected over 20 min at room temperature.

Disulfide reduction. This construct was created in three steps. (1) Var 4 and a truncated version of var 8 with a 3′ and a 5′ thiol, respectively, were reduced in 50 mM TCEP (BondBreaker Thermo Scientific). (2) These two oligonucleotides were linked by a disulfide. (3) The disulfide-bridged oligonucleotides were hybridized onto the DNA nanoswitch.

1. To reduce the thiols on the oligonucleotides, we incubated them in 50 mM TCEP for 1 h at RT.
2. Equal volumes of the two oligonucleotide-TCEP mixtures were then combined. The TCEP was removed using a Qiagen nucleotide-removal kit. The oligonucleotides were then allowed to form disulfides in the absence of reducing agent in PBS for 1 h before the products were run on a precast 4–20% gradient polyacrylamide TBE gel. As the oligonucleotides were different sizes (60 and 30 nt), the appropriate heterodimer could be easily identified and purified using electroelution as previously described[5].
3. The var 4-S-S-var 8 was used instead of the normal var 4 and var 8. This was annealed onto the linear M13 backbone at a 1:1 ratio and was added along with the other oligonucleotides at the beginning of the annealing. This yielded loops with a disulfide bridging variable regions 4 and 8.

With these loops in hand, we could observe loop opening as a result of TCEP reduction of the disulfide bond. To accomplish this, we mixed equal volumes of 20 μM TCEP and 160 nM loops, both of which were diluted in NEB buffer 2, at different time points before running the gel. Seven time points were collected over 10 d at room temperature before running the gel.

Multistate loops. The bispecific receptor was formed by using a lightning link kit (Innova Biosciences) to attach streptavidin to sheep polyclonal anti-dig (Roche 11333089001). The anti-dig, suspended in PBS, was added in a 1:1 ratio to the streptavidin, and the kit protocol was followed exactly. This was then diluted 1:1,250 into NEB buffer 2 with added 150 mM NaCl before use in forming multistate loops. The multistate loop was formed by using var 4 with a 3′ biotin, var 8 with a 5′ digoxigenin, and var 12 with 3′ digoxigenin in place of the normal var 4, 8, and 12 oligonucleotides. On-rate and off-rate measurements were performed using the same procedure used for the biotin-streptavidin experiments with slight modifications. Rather than adding streptavidin, we added the diluted bispecific receptor, and samples were quenched with 2 μL of 5 μM digoxigenin-functionalized oligonucleotide (an oligonucleotide was used, as digoxigenin is not water soluble) suspended in a saturated biotin solution. Gels were run at 6.25 V cm^{-1} for 125 min with buffer chilled to 4 °C before running.

Gel image analysis. We analyzed gel images in one of two ways.

1. All non-multistate gels (with only two bands) were analyzed in the following way. The amount of material in each gel band was quantified by analyzing the scanned gel images with the gel analysis tool in the freely available ImageJ software package. Using rectangular regions of interest that capture just the width of the gel bands, this toolbox produces intensity profiles whose area can be measured to quantify the total brightness in each band. We applied the same rectangular window size to each lane within a single gel. In many gels the highest–molecular

weight band of the added ladder was used as a normalizing reference lane. This relaxed the constraints of pipetting perfectly across all lanes.

2. All multistate gels (with five bands) were analyzed as follows. A custom Matlab interface, available upon request, was developed for fitting the intensity profiles of the imaged gel bands. The software interface was modeled after the ImageJ interface. Rectangular boxes were drawn around each lane to define a region of interest. Median filtering is a common technique used to remove speckle noise in images. Rather than filtering the entire image, each individual lane was median filtered by row to remove speckle noise without sacrificing resolution in the direction of band migration. After plotting the median-intensity profile, we subtracted the background using a 4- to 6-point piecewise linear function to outline the background. The background was found to be very similar across lanes, and often the same background profile could be subtracted from the majority of the lanes. Once the profiles were extracted, least-squares fitting of each profile to the model was performed in Matlab. Individual bands run on their own show a skewed Gaussian profile, also known as a skew normal distribution, with a skew parameter of ~−2.5 (**Supplementary Fig. 5**). Thus, the entire multistate median-intensity profile (from just above the highest band to just below lowest) was fit using a sum of five skewed Gaussians. A common skew parameter was used for all five bands, and a common initial guess of band width was used with a fitting range of ±10 pixels. These input parameters allowed for converging fits across all lanes and resulted in fits that closely matched the observed intensity profiles (**Fig. 3a**). The areas of the individual bands were calculated by integrating the individual skewed Gaussians. Error in the fitted areas was estimated by calculating the areas within the 1σ confidence interval of the fit parameters. These areas were all normalized by the total area (the sum of all of the skewed Gaussian areas). The identities of the bands were validated by analyzing gels in which individual loop sizes were formed (**Supplementary Fig. 5**). Accuracy of band quantification was confirmed by mixing these individual loops in known ratios—the measured values of the individual bands were found to be within 10% of their true values.

We used the following equation for a skew normal/skewed Gaussian distribution

$$Ae^{-\left(\frac{x-b}{c}\right)^2}\left(1+\mathrm{erf}\left(a\frac{x-b}{c}\right)\right)$$

Data analysis. On the basis of a gel we ran to establish repeatability of pipetting and imaging, we conservatively estimate the error per lane at ±5% plus the detection limit (which will vary by imager). For lanes that used a reference band to normalize brightness, the 5% error per band was propagated to yield roughly 7% error per measurement. Error bars were produced on the basis of this analysis, and all fitting procedures used an error-weighted least-squares fit. Timed pipetting for on-rate experiments was conservatively assumed to have an error of 2 s, which was propagated to overall y-error by multiplying by the derivative of a preliminary fit.

Model. The time evolution of DNA nanoswitch states are modeled using multistep reaction kinetics. On rates are modeled as a two-step process

Unbound linear → Singly bound linear → Looped

Step 1 represents the binding of a free receptor in solution to a ligand on the scaffold (yielding the solution on-rate); step 2 represents the subsequent binding of this receptor to another ligand on the same scaffold to form a loop (yielding the loop-closure rate). On-rate and off-rate models for both the two-state and five-state systems are detailed in **Supplementary Note 1**.

Thermodynamic analysis. The dissociation constant K_D was determined by the ratio of the off- and on-rates, and the equilibrium free energy ΔG^0 was determined by

$$\Delta G^0 = -RT\ln(\tilde{K}_D)$$

where R is the gas constant, T is the absolute temperature, and the dissociation constant, which is determined by dividing the off-rate by the on-rate and is made dimensionless by dividing it by a reference concentration, i.e., $\tilde{K}_D = K_D/(1M)$. We additionally used Eyring analysis to fit the temperature dependence of the kinetic rates

$$\ln\left(\frac{k}{T}\right) = \frac{-\Delta H}{R}\left(\frac{1}{T}\right) + \ln\left(\frac{k_B}{h}\right) + \frac{\Delta S}{R}$$

where k is the kinetic rate constant, k_B is the Boltzmann constant, h is Planck's constant, and ΔH and ΔS are the enthalpy and entropy of activation, respectively.

For the salt dependence, we used the kinetic salt relationship

$$\log(k) = \log(k_0) + 2A \times Z_A \times Z_B\sqrt{I}$$

where k is the kinetic rate constant, k_0 is the rate constant without the salt, A is the Debye-Hückel constant, Z_A and Z_B are the charges on the two interacting species, and I is the ionic strength of the solution (**Supplementary Note 2**).

17. Strunz, T., Oroszlan, K., Schäfer, R. & Güntherodt, H.J. *Proc. Natl. Acad. Sci. USA* **96**, 11277–11282 (1999).

doi:10.1038/nmeth.3209

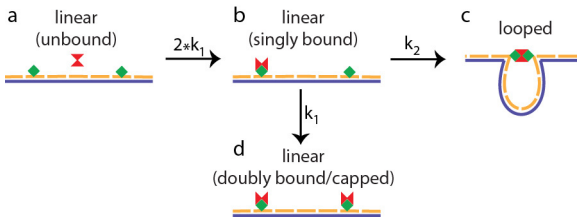

Supplementary Figure 1

Graphical representations of kinetic model.

The linear unbound construct (a) has two free ligands (green). The two free ligands result in the receptor (red) binding with twice its solution on-rate ($2*k_1$) to form the singly bound state (b). This now singly bound construct can either form a loop (c) by the same receptor binding to the second ligand at some loop closure rate (k_2), or a second receptor can bind to the scaffold at the receptor solution-on-rate (k_1) resulting an a doubly bound, or capped state (d).

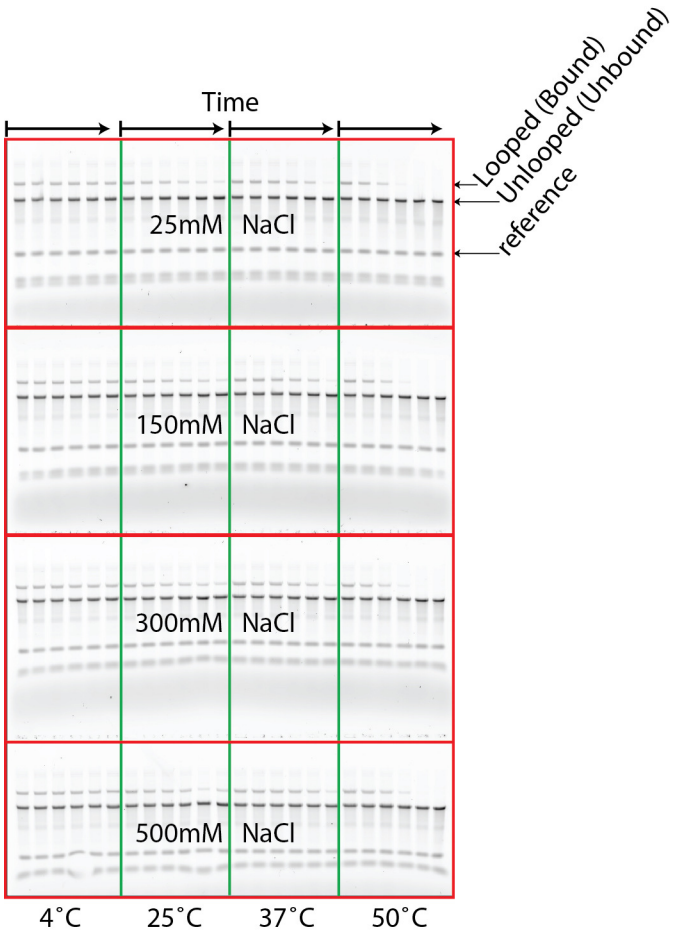

Supplementary Figure 2

Parallel measurements: biotin-streptavidin exploring a broad range of experimental conditions.

A highly parallel biotin-streptavidin off-rate measurement where an array of 16 different experimental conditions with 6 time points each were tested on a single 96-lane gel. Each of the 4 combs corresponds to a different salt condition, and within each comb experiments were conducted at 4 different temperatures. The band below the linear band is thought to be the result of enzyme promiscuity during the linearization process, and all lower bands result from the addition of a ladder used as a reference band to help alleviate the effects of pipetting error.

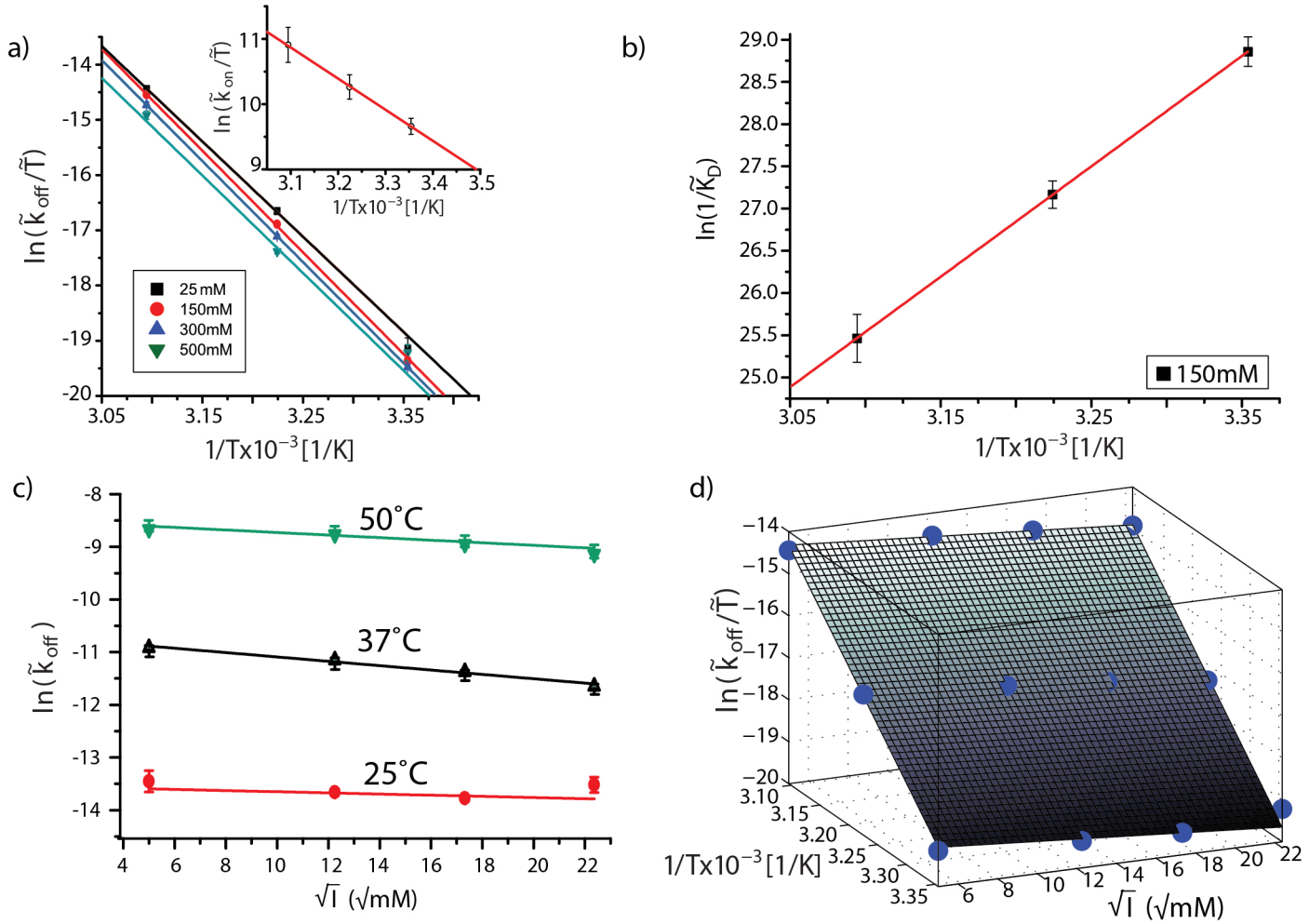

Supplementary Figure 3

Temperature and salt dependence of biotin-streptavidin interaction kinetics.

a) Eyring plot of the temperature dependence of the off-rate shows similar slopes for each salt condition but varying offsets. The off-rate and temperature were made dimensionless by scaling them by our reference units, i.e $\tilde{k}_{\text{off}} = \frac{k_{\text{off}}}{1s^{-1}}$ and $\tilde{T} = \frac{T}{1K}$. Fits were performed for data in the temperature range 25˚C to 50˚C Inset shows the temperature dependence of the on-rates. Inset shows Eyring analysis of on rates over the same temperature range of 25˚C to 50˚C. From linear fits to these data we obtain a transition-state enthalpies of $\Delta H^{\ddagger}_{on}$ = 9.48 ± 0.18 kcal/mol, and $\Delta H^{\ddagger}_{off}$ = 36.64 ± 0.50 kcal/mol b) Van't Hoff plot from 25˚C to 50˚C. The dissociation constant was made dimensionless by scaling it by our reference units, i.e $\tilde{K}_{\text{D}} = K_{\text{D}}/(1M^{-1})$. The red curve indicates a linear fit to the data. The fit was of the form $\ln\left(\frac{1}{\tilde{K}_D}\right) = \frac{\Delta S}{R} - \frac{\Delta H}{R} \cdot \frac{1}{T}$, where R is 1.99 x 10^{-3} kcal K^{-1} mol^{-1}, and T is the absolute temperature in K. This fit yielded the following values: ΔH = -26.01 ± 0.05 kcal mol^{-1}, and ΔS = -0.0298 ± 0.0002 kcal K^{-1} mol^{-1}. c) Plot showing salt dependence, again with similar slopes across all temperature conditions but with varying offsets. d) a 3D plot of the data fit with a least squares surface. All error bars represent the propagated error in the values taken from **Supplementary Table 2**.

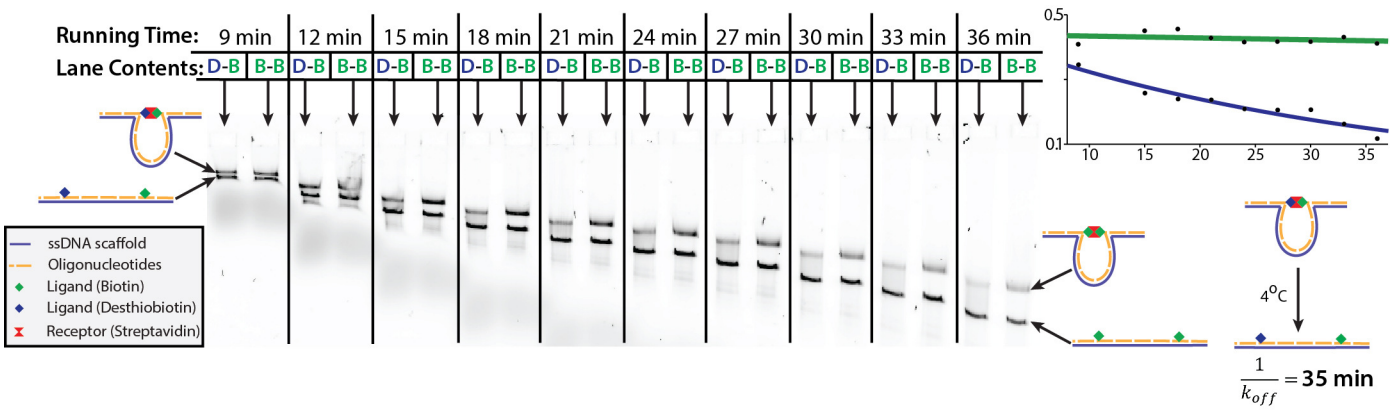

Supplementary Figure 4

Measurement of weak interactions.

The nanoswitches have proven very useful for the study of strong interactions. To extend the range of interactions which could be studied we modified the gel running procedure (see online methods). Noting that reptation of the DNA through the gel matrix acts as a quencher by preventing open loops from closing we are able to monitor the ratio of looped to unlooped as a function of time run in a gel. To indicate the location of the looped band a nanoswitch with a negligible off rate was run alongside each time point. A desthiobiotin-streptavidin-biotin (D-B) bridge was used for the weak interaction, and a biotin-streptavidin-biotin (B-B) bridge was used as the strong interaction. The B-B nanoswitches stayed relatively unchanged as a function of running time. The D-B constructs however show significant decay which was fit with a single exponential yielding a time constant of 35.3 ± 7.5 minutes.

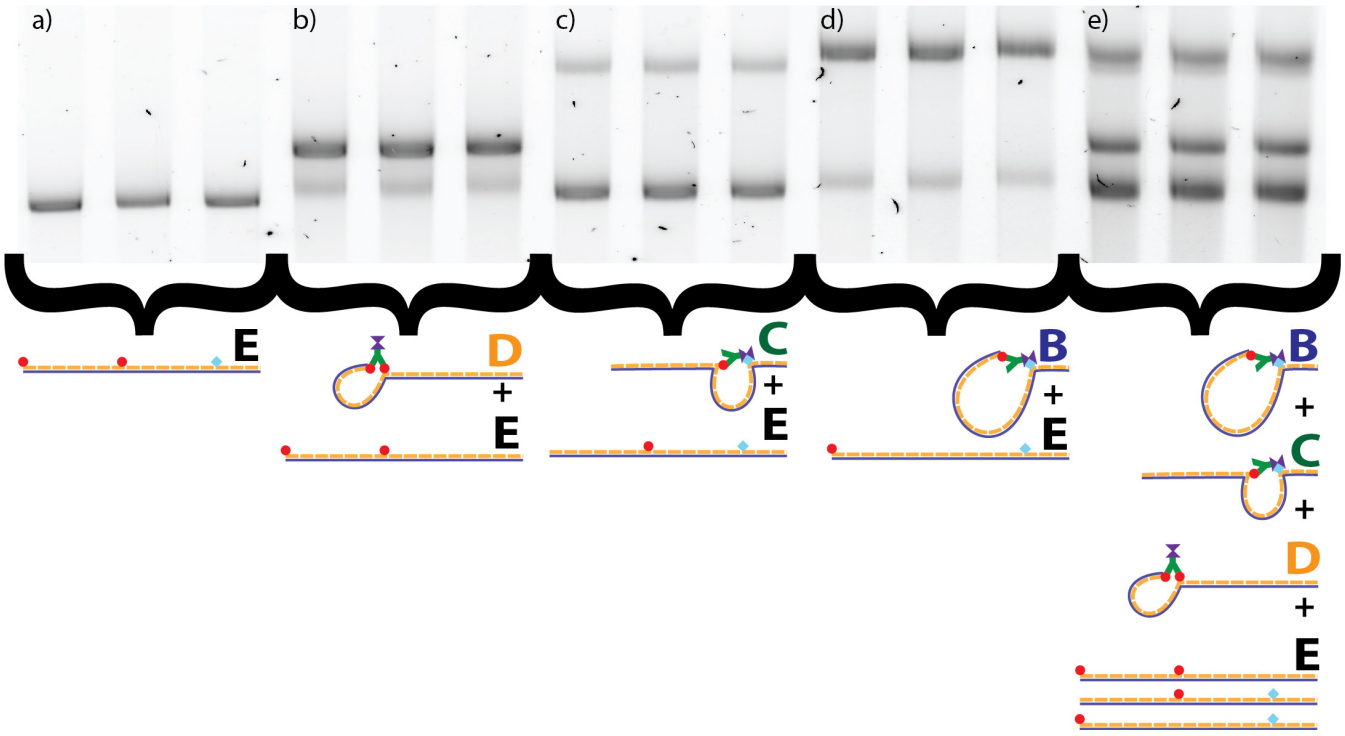

Supplementary Figure 5

Multistate band verification.
To determine the location of the bands which represent the different states of the bispecific receptor binding to the trifunctionalized nanoswitch, we made nanoswitches capable of forming one or a subset of states (each set was run in triplicate). a) trifunctionalized nanoswitches without the bispecific receptor result in only a linear band (E). b) Nanoswitches with both digoxigenin functionalizations but lacking the biotin can form the E and D states. c) Nanoswitches lacking the terminal digoxigenin can form the E and C states. d) Nanoswitches lacking the central digoxigenin can form the E and B states. e) In this lane the samples from the lanes in b, c, and d were mixed in a 1:1:1 volumetric ratio before running on the gel to simulate the conditions seen in the multistate experiments. Note that it was not possible to make a construct which could exclusively form state A in Figure 3 but this state is attributed to the only remaining band, and selective quenching experiments (data not shown) indicate that this construct contains both digoxigenin and biotin dependent interactions which collapse into the appropriate states upon quenching exclusively with digoxigenin or biotin.

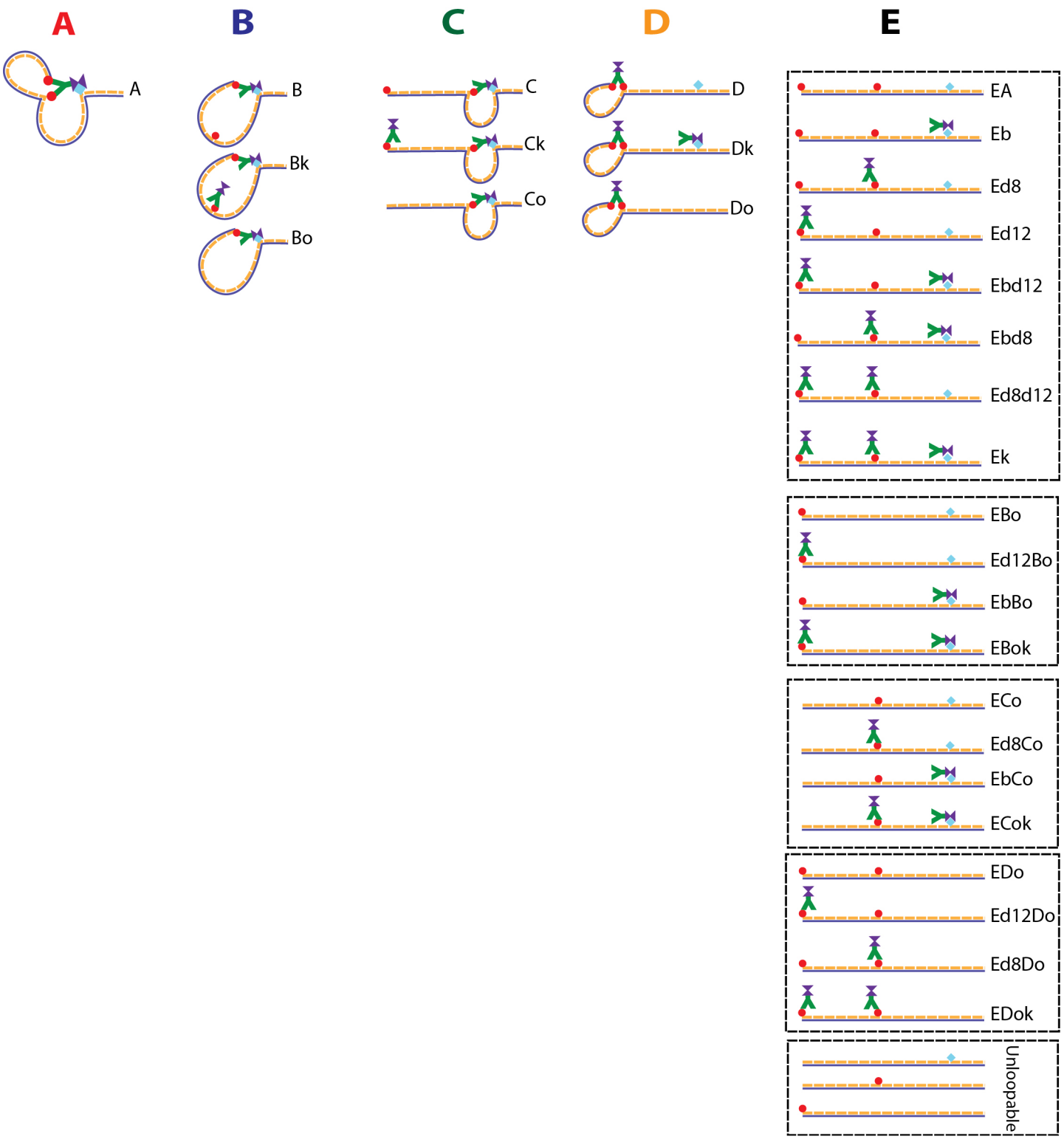

Supplementary Figure 6

Multistate-model states.
The model consists of 33 accessible states that can be occupied by the system. These 33 states are read out as 5 discrete gel bands, corresponding to 5 topological states indicated by the bold letters **A**, **B**, **C**, **D**, and **E**. **A** consists of only one state. Although bands **B**-**D** each represent one topological state, they are each composed of three states: 1) A piece of DNA in topological state **B**, **C**, or **D** that can

transition into topological state **A**, 2) A piece of DNA in topological state **B**, **C**, or **D** that cannot transition into topological state **A**, because the remaining ligand is capped by a second bispecific receptor, 3) A piece of DNA in topological state **B**, **C**, or **D** that cannot transition into topological state **A** because the DNA nanoswitch is missing the third ligand. The E state consists of 23 states. The boxes from top to bottom indicate linear states accessible when: all three ligands are present; the two digoxigenin ligands are present; the central digoxigenin ligand, and the biotin are present; the terminal digoxigenin ligand, and the biotin are present; only one ligand is present. This final set of three linear constructs, and the last construct in each box cannot form loops.

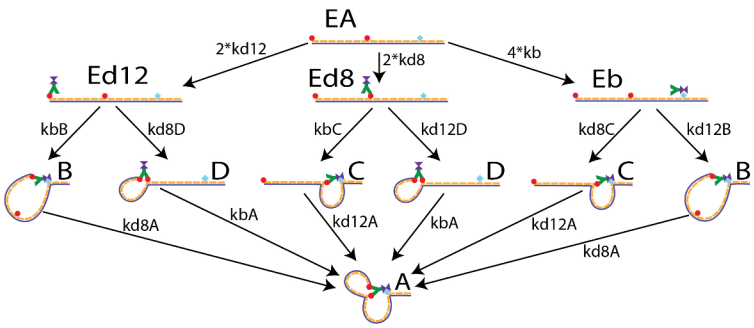

Rate Constant	Description	
kb	Per-site solution on rate for biotin	
kd8	Per-site solution on rate for the dig on var 8	
kd12	Per-site solution on rate for the dig on var 12	
Rate Constant	**Description**	**Definition**
kbC	Rate of biotin binding to form state C	$kbC = 4*kb*L_C$
kbB	Rate of biotin binding to form state B	$kbB = 4*kb*L_B$
kd8C	Rate of dig on var 8 binding to form state C	$kd8C = 2*kd8*L_C$
kd8D	Rate of dig on var 8 binding to form state D	$kd8D = kd8*L_D$
kd12B	Rate of dig on var 12 binding to form state B	$kd12B = 2*kd12*L_B$
kd12D	Rate of dig on var 12 binding to form state D	$kd12D = kd12*L_D$
kbA	Rate of biotin binding to form state A	$kbA = 4*kb*L_{DA}$
kd8A	Rate of dig on var 8 binding to form state A	$kd8A = kd8*L_{BA}$
kd12A	Rate of dig on var 12 binding to form state A	$kd12A = kd12*L_{CA}$

Supplementary Figure 7

Multistate on-rate kinetic model schematic.
The kinetic on-rate model consists of 3 solutions on rates and 6 effective loop concentrations resulting in effective on loop rate constants referred to as kbB, kbC, kd8C, kd8D, kd12B, kd12D, kbA, kd8A, and kd12A. The figure illustrates the kinetic model, excluding the capping phenomenon for clarity, and the table indicates the physical meaning and mathematical definition of each rate constant in the figure. The effective loop concentrations are as follows: L_B is the effective concentration between the biotin on var 4 and the dig on var 12, L_C is the effective concentration between the biotin on var 4 and the dig on var 8, L_D is the effective concentration between the dig on var 8 and the dig on var 12, L_{BA} is the effective concentration of the dig on var 8 relative to the var 4-var 12 complex, L_{CA} is the effective concentration of the dig on var 12 relative to the var 4-var 8 complex, L_{DA} is the effective concentration of the biotin on var 4 relative to the var 8-var 12 complex.

Technique	Equipment Cost[a]	Sample Cost[b]	Protein Usage[c]	Surface Free[c]
DNA Nanoswitches	**low**	**low**	**< 1ng**	**yes**
Surface Plasmon Resonance (SPR)	medium/high	medium	<10 µg	no
Nuclear Magnetic Resonance (NMR)	high	low	15-5000 µg	yes
Scintillation Proximity Assay (SPA)	medium	high	0.1-10 µg	yes
Fluorescence	medium/high	low/medium	1 µg	yes
Bio-Layer Interferometry (BLI)	medium	medium	< 1ng	no
Quartz crystal microbalance (QCM)	medium	low	< 1ng	no
Isothermal calorimetry (ITC)	high	low	0.1-0.4 mg	yes

[a] low: <$5k, medium: $5-$50k, high: >$50k

[b] low: <$0.1, medium: $0.1-$1, high: >$1

[c] Most values taken from Table 1.1 in A. Dejaegere, et. al.

Supplementary Table 1: Comparison of biomolecular interaction analysis techniques

	Units	Condition	Our values	Literature Range	References
off-rate	1/s	25˚C	**(1.2 ± 0.1) x 10^{-6}**	1.4 x 10^{-6} to 5.4 x 10^{-6}	Green, 1990; Piran, 1990; Chilkoti, 1995; Klumb, 1998; Hyre, 2006; Levy, 2008; Deng, 2012
		37˚C	**(1.4 ± 0.1) x 10^{-5}**	2.9 x 10^{-5} to 6.8 x 10^{-5}	Hyre, 2000; Howarth, 2006; Chivers, 2010; Magalhaes, 2011
on-rate*	1/(M*s)	25˚C	**(4.0 ± 0.7) x 10^{6}**	1.4 x 10^{6} to 8.5 x 10^{7}	Burunda, 1999; Qureshi, 2001; Hyre, 2006; Srisa-Art, 2008; Takakura, 2009; Magalhaes, 2011
		37˚C	**(9.0 ± 1.4) x 10^{6}**	5.5 x 10^{7} to 6.7 x 10^{7}	Chivers, 2010; Magalhaes, 2011
ΔH	kcal/mol	25˚C	**-26 ± 0.1**	-24.5 to -29.4	Chilkoti, 1995; Klumb, 1998; Hyre, 2000; Magalhaes, 2011
ΔG	kcal/mol	25˚C	**-17.1 ± 0.1**	-16.7 to -18.9	Green 1990; Chilkoti, 1995; Qureshi, 2001; Hyre, 2006; Magalhaes, 2011
		37˚C	**-16.7 ± 0.1**	-16.3 to -16.8	Chivers, 2010; Magalhaes, 2011
K_d	1/M	25˚C	**(2.9 ± 0.5) x 10^{-13}**	1.4 x 10^{-14} to 5.5 x 10^{-13}	Green, 1990; Chilkoti, 1995; Qureshi, 2001; Hyre, 2006; Magalhaes, 2011
		37˚C	**(1.6 ± 0.3) x 10^{-12}**	6.0 x 10^{-13} to 1.0 x 10^{-12}	Chivers, 2010; Magalhaes, 2011

*Our on-rates are reported per molecule of streptavidin. Literature range may contain a mixture of both per molecule and per binding site on rates as it is rarely specified.

Notes: 1) References that quoted either K_d or ΔG were included in both parameters using the relationship $\Delta G = RT*\ln(K_d)$

2) References that measured the on and off rates were included in both K_d (k_{off}/k_{on}) and ΔG

Supplementary Table 2: Comparison of our kinetic and thermodynamic values for the biotin-streptavidin interaction to those in previously-published works.

	k_{off} (10^{-7} s^{-1})			
Sample (Salt conc.)	**4°C**	**25°C**	**37°C**	**50°C**
Streptavidin (25mM)	2.02±0.22	14.38±2.92	181.8±7.6	1725±67
Streptavidin (150mM)	2.77±0.68	11.66±0.70	143.8±5.8	1565±25
Streptavidin (300mM)	2.84±0.60	10.39±0.51	115.1±3.6	1299±68
Streptavidin (500mM)	0.64±0.37	13.45±1.99	87.5±3.8	1073±81
Avidin (150mM)	--	2.25±0.32	45.6±10.3	--
Neutravidin (150mM)	--	1.84±0.83	91±23	--

	k_{on}/molecule[b] (10^{6} M^{-1} s^{-1})			
Sample (Salt conc.)	**4°C**	**25°C**	**37°C**	**50°C**
Streptavidin (150mM)	1.7±0.4	4.0±0.7	9.0±1.4	17.9±5.1
Avidin (150mM)	--	6.21±0.24[a]	18.86±2.0[a]	--
Neutravidin (150mM)	--	0.37±0.27	1.47±0.42	--

	Equilibrium properties (150mM NaCl) Per Molecule			
Measurement	**4°C**	**25°C**	**37°C**	**50°C**
Streptavidin K_D (10^{-14} M)	16.1±5.6	29.4±5.1	159.5±26	870±248
Streptavidin ΔG^0 (kcal/mol)	-16.2±.2	-17.1±0.1	-16.7±0.1	-16.4±0.2
Avidin K_D (10^{-14} M)	--	3.6±0.5[a]	24.2±6.0[a]	--
Avidin ΔG^0 (kcal/mol)	--	-18.3±0.1[a]	-17.9±0.2[a]	--
Neutravidin K_D (10^{-14} M)	--	49±42	617±236	--
Neutravidin ΔG^0 (kcal/mol)	--	-16.8±0.5	-15.9±.2	--

[a]Non-specific avidin interactions may result in additional uncertainty in k_{on}

[b]Divide these k_{on} measurments by 4 to get the k_{on} per binding site

Supplementary Table 3: Kinetic and thermodynamic values obtained from studying the interactions of biotin with Streptavidin, Avidin, and Neutravidin. Errors indicate the 67% confidence interval on the fit parameters (a 3 parameter model fit to 6 data points for each condition).

Parameter	kb on	kb off	kd on	kdoff	kd8 on	kd12 on	kd8 off	kd12 off	L_B	L_C	L_D	L_{BA}	L_{CA}	L_{DA}
Units	10^6 /$M^{-1}s^{-1}$	$days^{-1}$	10^6 /$M^{-1}s^{-1}$	$days^{-1}$	10^6 /$M^{-1}s^{-1}$	10^6 /$M^{-1}s^{-1}$	$days^{-1}$	$days^{-1}$	10^{-9} M	10^{-9} M	10^{-9} M	10^{-9} M	10^{-9} M	10^{-9} M
Upper Bound	0.12	2.08	5.24	1.85	2.69	5.24	1.82	1.85	27.45	11.33	245.31	19.51	30.76	35.98
Average	**0.10**	**2.05**	**2.65**	**1.81**	1.62	2.24	1.80	1.82	15.51	10.85	112.32	15.28	7.84	31.02
Lower Bound	0.09	2.01	1.15	1.77	1.15	1.54	1.77	1.80	11.14	10.39	90.12	11.45	4.30	28.26

Supplementary Table 4. Results from multistate on-rate and off-rate fits, where L_B is the effective concentration between the biotin on var 4 and the dig on var 12, L_C is the effective concentration between the biotin on var 4 and the dig on var 8, L_D is the effective concentration between the dig on var 8 and the dig on var 12, L_{BA} is the effective concentration of the dig on var 8 relative to the var 4-var 12 complex, L_{CA} is the effective concentration of the dig on var 12 relative to the var 4-var 8 complex, L_{DA} is the effective concentration of the biotin on var 4 relative to the var 8-var 12 complex. Additionally, to verify that the solution on-rate measurements are independent of how we scaffold the ligands, we redid the measurements using a construct containing two biotin molecules and a single digoxigenin molecule, and found that these solution on-rates were in close agreement with our prior measurements (data not shown).

Streptavidin concentration (nM)	Solution on-rate (10^6 M^{-1} s^{-1}) (per binding site)
1	1.15 ± 0.18
3	1.00 ± 0.09
10	0.88 ± 0.10
Mean	1.01 ± 0.08

Supplementary Table 7. Solution on-rate is independent of loop size. Solution on-rate values reported are the weighted means of 3 experiments with the errors being the weighted standard deviation. The mean value is the mean of the solution on-rates from the four different ligand positions with the error given by the standard error of the mean. All values are reported as a per-binding site on-rate. To get the per-molecule on-rate, one would need to divide these values by one molecule per four binding sites (i.e. multiply by 4).

Ligand Positions	Solution on-rate (10^6 M^{-1} s^{-1}) (per binding site)
4-8	1.03 ± 0.15
8-12	1.34 ± 0.28
4-12	1.06 ± 0.29
1-12	1.75 ± 0.21
Mean	1.29 ± 0.17

Supplementary Table 8. Solution on-rate is independent of receptor concentration. Solution on -rate values reported are the solution on-rate fit parameter from an error weighted fit of 10 data points with a 3 parameter model. The errors for measurements are the one-sigma confidence intervals of the fit parameter. The mean value is the mean of the solution on-rates from the three different concentrations with the error given by the standard error of the mean. All values are reported as a per-binding site on-rate. To get the per-molecule on-rate, one would need to divide these values by one molecule per four binding sites (i.e. multiply by 4).

Supplementary Note 1: Kinetic Models

Two-state kinetic model

For off-rate measurements of two-band systems, the data was fit to a single exponential decaying to zero. In the case of biotin-streptavidin measurements, the time constants were multiplied by two since each streptavidin has two pathways to cause the loop to dissociate. For on-rate measurements of two-band systems, we used a kinetic model consisting of 4 states and two kinetic rate constants. Reverse rates were not considered to play a role since they were many orders of magnitude slower. This model results in a nonlinear system of differential equations that can be solved numerically (using NDsolve in Mathematica, for example). In our case, however, we were able to reduce these to a linear system of differential equations by using the assumption that the concentration of streptavidin is constant, which is a good approximation for our experimental conditions since the streptavidin was at a much higher concentration than the biotin-looped construct (3nM vs. 80pM). Furthermore, we validated this approximation by comparing our results with the full numerical solution, and saw no discernable differences. Thus, the effective system of differential equations for the on-rate measurements is:

$$
\begin{aligned}
a'(t) &= -S \cdot k_1 \cdot 2a(t) \\
b'(t) &= S \cdot k_1 \cdot \big(2a(t) - b(t)\big) - k_2 \cdot b(t) \\
c'(t) &= k_2 \cdot b(t) \\
d'(t) &= S \cdot k_1 \cdot b(t)
\end{aligned}
$$

Where a(t) is the concentration of unlooped construct with no ligands bound, b(t) is the concentration of unlooped construct with only one ligand bound to one receptor, c(t) is the concentration of looped construct with two ligands bound to a single common receptor molecule, d(t) is concentration of unlooped construct with both ligands bound to different receptor molecules, S is the concentration of streptavidin, and k_1 and k_2 are the per-site kinetic rates for streptavidin binding from solution and loop closure, respectively (accounting for the fact that in solution streptavidin has 4 binding sites, and after binding there are only 3 avaliable binding sites for loop closure). Note that k_2 does not depend on the concentration of strepavidin in solution, since the loop closure rate is governed by an effective local concentration within the nanoswitch that is set by the loop length. This system of equations results in an analytical expression:

$$
c(t) = \frac{A_o[3k_2 - 3k_2 e^{-8k_1 St} - 4k_1 S - 4k_1 S e^{-8k_1 St} + 8k_1 S e^{(-3k_2 - 4k_1 S)t}]}{(3k_2 - 4k_1 S)}
$$

$$
A_o = \lim_{t \to \infty} c(t)
$$

Nature Methods: doi:10.1038/nmeth.3209

C(t) was fit to the data with three free parameters, k_1, k_2, and Ao. In the regime of concentrations that we used (local biotin > free streptavidin > nanoswitches), the on-rate fitting was less sensitive to k_2 than k_1, and constraining k_2/k_1 for the fits resulted in solution on-rates that overlapped within error with fits using k_1 and k_2 as free parameters.

This model allows for the determination of both the solution on-rate, which is independent of the polymer looping kinetics, and the loop closure rate as illustrated in **Supplementary Figure 4**.

Additionally, to examine the effect of ligand placement on the determination of the solution on-rate, we conducted biotin-streptavidin on-rate experiments with a variety of ligand positions at room temperature. The results, shown in **Supplementary Table 7**, indicate that the solution on-rate measurements are in reasonable agreement, exhibiting a relative standard error of the mean (1.29×10^6 M^{-1} s^{-1}) of 13%.

To further test the robust nature of the system we analyzed the effect of keeping the ligand positions constant while altering the concentration of the receptor (see **Supplementary Table 8**). We found that the measured solution on-rates are in reasonable agreement even when varying the receptor concentrations by an order of magnitude, yielding a relative standard deviation of 13%. Note that working outside this range may be difficult as protein concentrations become unreliable below 1 nM, and the rate of loop formation becomes very fast above 10 nM (see online methods for details).

Multistate off-rate model

For off-rate measurements of multistate (5 band) systems we used a model consisting of 5 topological states and 3 rate constants. Reverse rates were not considered to play a role as the presence of excess quencher prevents the closure of loops. This model results in a linear system of differential equations.

$$\mathbf{A}'(t) = -(kb + kd8 + kd12) * \mathbf{A}(t)$$

$$\mathbf{B}'(t) = kd8 * A(t) - (kb + kd12) * \mathbf{B}(t)$$

$$\mathbf{C}'(t) = kd12 * A(t) - (kb + kd8) * \mathbf{C}(t)$$

$$\mathbf{D}'(t) = kb * A(t) - (kd8 + kd12) * \mathbf{D}(t)$$

$$\mathbf{E}'(t) = (kb + kd12) * \mathbf{B}(t) + (kb + kd8) * \mathbf{C}(t) + (kd8 + kd12) * \mathbf{D}(t)$$

Where k_b is the biotin off rate, k_{d8} is the off rate of the digoxigenin on var 8, k_{d12} is the off rate of the digoxigenin on var 12, **A**(0)-**E**(0) are the starting fractions of construct in each state A-E illustrated in Figure 3. These differential equations can be easily solved analytically (for example, using Dsolve in Mathematica), resulting in the following set of equations:

$$\mathbf{A}(t) = \mathbf{A}(0)e^{(-kb - kd12 - kd8)t}$$

$$\mathbf{B}(t) = e^{(-kb - kd12 - kd8)t}(-\mathbf{A}(0)(e^{(kd8)t} - 1) + \mathbf{B}(0)e^{(kd8)t})$$

$$\mathbf{C}(t) = e^{(-kb - kd12 - kd8)t}(-\mathbf{A}(0)(e^{(kd12)t} - 1) + \mathbf{C}(0)e^{(kd12)t})$$

$$\mathbf{D}(t) = e^{(-kb - kd12 - kd8)t}(-\mathbf{A}(0)(e^{(kb)t} - 1) + \mathbf{D}(0)e^{(kb)t})$$

$$\begin{aligned}\mathbf{E}(t) = e^{(-kb - kd12 - kd8)t}&(\mathbf{A}(0)(2 - e^{(kb)t} - e^{(kd12)t} - e^{(kd8)t} + e^{(kb + kd12 + kd8)t}) \\ &+ \mathbf{B}(0)(e^{(kb + kd12 + kd8)t} - e^{(kd8)t}) + \mathbf{C}(0)(e^{(kb + kd12 + kd8)t} - e^{(kd12)t}) \\ &+ \mathbf{D}(0)(e^{(kb + kd12 + kd8)t} - e^{(kb)t}) + \mathbf{E}(0)e^{(kb + kd12 + kd8)t}\end{aligned}$$

These equations were then fit to the data using fminsearch to minimize the chi-squared in MATLAB with k_b, k_{d8}, k_{d12}, **A**(0), **B**(0), **C**(0), **D**(0), and **E**(0) as free parameters.

Multistate on-rate model

For the on-rate measurments of multistate (5 band) systems we used the model described below. This model results in a system of differential equations that can be solved numerically (using ODE15s in matlab, for example) with the following assumptions: The reverse rates were not considered to play a role since they were many orders of magnitude slower, and the concentration of the bispecific receptor is considered to be constant, which is a good approximation for our experimental conditions since the bispecific receptor was at a much higher concentration than the nanoswitches (3nM vs. 80pM).

The on rate model is schematized generally in the figures s5 and s6, followed by the differential equations that comprise the model.

Models were fit to experimental data using fminsearch in matlab to find the minimum of the χ^2:

$$X^2 = \sum_{i=1}^{N} \frac{(y_i^{exp} - y_i^{model})}{\sigma_i^2}$$

y_i^{exp} is the ith experimental data point. y_i^{model} is the theoretical prediction given by the model of the ith data point, and σ_i^2 is the variance in the ith experimental data point.

To estimate errors on the fit parameters obtained using fminsearch, we calculated the local curvature of the χ^2as a function of each fit parameter. The variance of the fit parameter is estimated by $(\sigma_{xi})^2 = 2\left(\frac{\delta^2 X^2}{\delta x_i^2}\right)^{-1}$ where x_i is the ith fit parameter.

Multistate on-rate model details

In addition to loop formation our model accounts for the presence of scaffolds that lack one or more ligand, and for the phenomenon of capping, in which two or more receptor molecules bind to a single scaffold. The model assumes that the concentration of the bispecific receptor molecule, S, is constant, as it is in great excess compared to the scaffold. Additionally, as the time scales for the on rate are much smaller than those for the off rate, the model assumes no unbinding events occur during loop formation.

Bold letters **A**, **B**, **C**, **D**, and **E** represent topological states composed of the individual states, illustrated in figure s5, as follows:

$$\mathbf{A}(t) = A(t)$$

$$\mathbf{B}(t) = B(t) + Bk(t) + Bo(t)$$

$$\mathbf{C}(t) = C(t) + Ck(t) + Co(t)$$

$$\mathbf{D}(t) = B(t) + Dk(t) + Do(t)$$

$$\mathbf{E}(t) = EA(t) + Eb(t) + Ed8(t) + Ed12(t) + Ebd8(t) + Ebd12(t) + Ed8d12(t) + Ek(t) + EBo(t) + Ed12Bo(t) + EbBo(t) + EBok(t) + ECo(t) + Ed8Co(t) + EbCo(t) + ECok(t) + EDo(t) + Ed12Do(t) + Ed8Do(t) + EDok$$

A linear piece of DNA that has all three ligands, and therefore has the ability to enter state A, is referred to as being in state EA.

Molecules can transition from state EA into either state Eb, Ed8, or Ed12 indicating a linear strand of DNA with a receptor bound to the biotin, var 8-dig, or var 12-dig respectively. Additionally molecules can transition out of these states either by binding a second receptor, or by forming a loop as indicated by the following equations:

$$Eb'(t) = 4\ kb\ \ S\ \ EA(t) - (\ kd12B + kd8C\ )\ \ Eb(t) - 2\ \ kd8\ \ S\ \ Eb(t) - 2\ \ kd12\ \ S\ \ Eb(t)$$

$$Ed8'(t) = 2 * kd8 * S * EA(t) - (\ kbC + kd12D\ ) * Ed8(t) - 4 * kb * S * Ed8(t) - 2 * kd12 * S * Ed8(t);$$

$$Ed12)'(t) = 2 * kd12 * S * EA(t) - (\ kbB + kd8D\ ) * Ed12(t) - 4 * kb * S * Ed12(t) - kd8 * 2 * S * Ed12(t);$$

Where kb, kd8, and kd12 are the per-site solution on rates for biotin, the dig on var 8, and the dig on var 12 respectively, and S is the concentration of the bi-specific receptor, assumed to be constant in time.

The formation of linear constructs with two receptor molecules bound can be modeled with the following equations:

$$Ebd8'(t) = 2 * kd8 * S * Eb(t) + 4 * kb * S * Ed8(t) - (kd12D + kd12B + 2 * kd12 * S) * Ebd8(t);$$

$$Ebd12'(t) = 2 * kd12 * S * Eb(t) + 4 * kb * S * Ed12(t) - (kd8C + kd8D + 2 * kd8 * S) * Ebd12(t);$$

$$Ed8d12'(t) = 2 * kd12 * S * Ed8(t) + kd8 * 2 * S * Ed12(t) - (kbC + kbB + 4 * kb * S) * Ed8d12(t);$$

Where Ebd8 indicates a linear scaffold with a receptor molecule bound to the biotin and a receptor molecule bound to the dig on var 8, Ebd12 indicates a linear scaffold with a receptor molecule bound to the biotin and a receptor molecule bound to the dig on var 12, Ed8d12 indicates a linear scaffold with a receptor molecule bound to the dig on var 8, and a receptor molecule bound to the dig on var 12

The linear EA state can also be capped by 3 separate receptor molecules.

$$Ek'(t) = 2 * kd12 * S * Ebd8(t) + 2 * kd8 * S * Ebd12(t) + 4 * kb * S * Ed8d12(t);$$

A linear piece of DNA that is missing one ligand cannot form state A. These linear pieces of DNA are referred to by the highest order loop they can form. Thus, a scaffold that only has a biotin on var 4 and a dig on var 12, and can therefore only form loop B, is referred to as EBo; a scaffold that only has a biotin on var 4 and a dig on var 8, and therefore can only form loop C, is referred to as ECo; a scaffold that only has a dig on var 8 and a dig on var 12, and can therefore only form loop D, is referred to as EDo.

Molecules can transition from state EBo into either state EbBo, or Ed12Bo indicating a linear molecule with a receptor bound to the biotin, or var 12-dig respectively. Additionally molecules can transition out of these states either by binding a second receptor, or by forming a loop as indicated by the following equations:

$$EbBo'(t) = 4 * kb * S * EBo(t) - kd12B * EbBo(t) - 2 * kd12 * S * EbBo(t);$$

$$Ed12Bo'(t) = 2 * kd12 * S * EBo(t) - kbB * Ed12Bo(t) - 4 * kb * S * Ed12Bo(t);$$

Molecules can transition from state ECo into either state EbCo, or Ed8Co indicating a linear molecule with a receptor bound to the biotin, or var 8-dig respectively. Additionally molecules can transition out of these states either by binding a second receptor, or by forming a loop as indicated by the following equation:

$$EbCo'(t) = 4 * kb * S * ECo(t) - kd8C * EbCo(t) - 2 * kd8 * S * EbCo(t);$$

$$Ed8Co'(t) = 2 * kd8 * S * ECo(t) - kbC * Ed8Co(t) - 4 * kb * S * Ed8Co(t);$$

Molecules can transition from state EDo into either state Ed8Do, or Ed12Do indicating a linear molecule with a receptor bound to the var 8-dig, or var 12-dig respectively. Additionally molecules can transition out of these states either by binding a second receptor, or by forming a loop as indicated by the following equation:

$$Ed12Do'(t) = 2 * kd12 * S * EDo(t) - kd8D * Ed12Do(t) - 2 * kd8 * S * Ed12Do(t);$$

$$Ed8Do'(t) = 2 * kd8 * S * EDo(t) - kd12D * Ed8Do(t) - 2 * kd12 * S * Ed8Do(t);$$

The following three equations represent scaffolds which have only two ligands, and become capped by the binding of two separate receptors.

$$EBok'(t) = 2 * kd12 * S * EbBo(t) + 4 * kb * S * Ed12Bo(t);$$

$$ECok'(t) = 2 * kd8 * S * EbCo(t) + 4 * kb * S * Ed8Co(t);$$

$$EDok'(t) = 2 * kd8 * S * Ed12Do(t) + 2 * kd12 * S * Ed8Do(t);$$

The rate of loop closure is described by the following equations.

$$A'(t) = kd8A * B(t) + kd12A * C(t) + kbA * D(t);$$

$$B'(t) = kd12B * Eb(t) + kbB * Ed12(t) - kd8A * B(t) - 2 * kd8 * S * B(t);$$

$$C'(t) = Eb(t) * kd8C + Ed8(t) * kbC - kd12A * C(t) - 2 * kd12 * S * C(t);$$

$$D'(t) = Ed8(t) * kd12D + Ed12(t) * kd8D - kbA * D(t) - 4 * kb * S * D(t);$$

Where kbB is the rate of biotin binding to form state B, kbC is the rate of biotin binding to form state C, kd8C is the rate of dig binding to var-8 form state C, kd8D is the rate of dig binding to var-8 form state D, kd12B is the rate of dig binding on var-12 to form state B, kd12D is the rate of dig binding on var-12 to form state D.

Loops which could transition into state A but are capped by having a second receptor molecule bind to the remaining ligand can be described as follows:

$$Bk'(t) = 2 * kd8 * S * B(t) + kd12B * Ebd8(t) + kbB * Ed8d12(t);$$

$$Ck'(t) = 2 * kd12 * S * C(t) + kd8C * Ebd12(t) + kbC * Ed8d12(t);$$

$$Dk'(t) = 4 * kb * S * D(t) + kd12D * Ebd8(t) + kd8D * Ebd12(t);$$

Where Bk, Ck, and Dk are the capped versions of Loops B, C, and D respectively.

Nature Methods: doi:10.1038/nmeth.3209

A linear piece of DNA that is missing one ligand cannot form state A. These linear pieces of DNA are referred to by the highest order loop they can form. Such that a scaffold that only has a biotin on var-4 and a dig on var-12, and can therefore only form loop B, is referred to as EBo; a scaffold that only has a biotin on var-4 and a dig on var-8, and therefore can only form loop C, is referred to as EBo; a scaffold that only has a dig on var-8 and a dig on var-12, and can therefore only form loop D, is referred to as Edo.

Bo′(t) = kd12B * EbBo(t) + kbB * Ed12Bo(t);

Co′(t) = kd8C * EbCo(t) + kbC * Ed8Co(t);

Do′(t) = kd12D * Ed8Do(t) + kd8D * Ed12Do(t);

Given these equations the amount of EA, EBo, ECo, and EDo can be described as follows:

EA(t) = EA_Start – Eb(t) – Ed8(t) – Ed12(t) – A(t) – B(t) – C(t) – D(t) – Ebd8(t) – Ebd12(t) – Ed8d12(t) – Ek(t) – Bk(t) – Ck(t) – Dk(t);

EBo(t) = EB_Start – EbBo(t) – Ed12Bo(t) – Bo(t) – EBok(t);

ECo(t) = EC_Start – EbCo(t) – Ed8Co(t) – Co(t) – ECok(t);

EDo(t) = ED_Start – Ed12Do(t) – Ed8Do(t) – Do(t) – EDok(t);

Multistate Kinetics Results:

Fitting the data with these on-rate and off-rate models, and using fminsearch to reduce the chi squared yielded the values reported in **Supplementary table 4** for the fit parameters.

Supplementary Note 2: Semiempirical formula for temperature and salt dependence

The temperature and salt dependence were analyzed using Eyring analysis and kinetic salt effect theory, respectively[9] (Supplemental Figure 1). Empirically, we found that these dependencies were separable over our measurement range, giving the following expression for the off-rate of DNA-linked biotin from streptavidin as a function of salt (25mM-500mM) and temperature (25°C-50°C):

$$\ln\left(\frac{k_{off}}{T}\right) \approx A + \frac{B}{T} + C\sqrt{I}$$

where k_{off} is the value of the off-rate in s^{-1}, T is the value of the absolute temperature in K, and I is the value of the ionic strength of the solution in mM. From a 2D least squares fit of our data, we found an offset A of 42.41 ± 1.7, an enthalpic prefactor B of -1.83 ± 0.06 x 10^4, and a salt dependence C of -0.033 ± 0.01. We note that the off rates used in developing this formula match off rates measured using a radiolabeled biotin-functionalized oligo under similar conditions, and are slower than the off rates measured using a free biotin.